Chemical Engineering Journal 380 (2020) 122530

Contents lists available at ScienceDirect

Chemical Engineering Journal

journal homepage: www.elsevier.com/locate/cej

Insight into mass transfer during ultrasound-enhanced adsorption/desorption of blueberry anthocyanins on macroporous resins by numerical simulation considering ultrasonic influence on resin properties

Yang Tao[a], Yue Wu[a], Yongbin Han[a,*], Farid Chemat[b], Dandan Li[a], Pau Loke Show[c]

[a] College of Food Science and Technology, Nanjing Agricultural University, Nanjing 210095, Jiangsu, China
[b] Université d'Avignon et des Pays de Vaucluse, INRA, UMR 408, GREEN Extraction Team, F-84000 Avignon, France
[c] Department of Chemical and Environmental Engineering, Faculty of Science and Engineering, University of Nottingham Malaysia, Jalan Broga, 43500 Semenyih, Selangor Darul Ehsan, Malaysia

HIGHLIGHTS

- Anthocyanin adsorption/desorption under sonication was modeled numerically.
- Diffusional models with changes of resin properties were robust for simulation.
- Values of k_L, D_s (adsorption) and D_e (desorption) increased with acoustic energy.
- Sonication increased surface diffusion contribution percentage to overall diffusion.
- High-intensity ultrasound attenuated anthocyanin concentration gradient within resins.

GRAPHICAL ABSTRACT

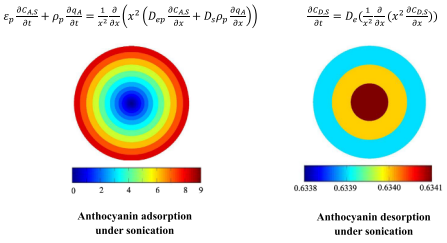

ARTICLE INFO

Keywords:
Ultrasound
Adsorption/desorption
Anthocyanins
Mass transfer
Diffusional modeling

ABSTRACT

The mass transfer mechanism about ultrasonic enhancement of blueberry anthocyanin adsorption and desorption on macroporous resins were investigated. Ultrasound treatment led to the decrease of resin size, whereas average pore diameter, specific surface area, total pore volume were less affected. Then, the pore volume and surface diffusion model considering ultrasound-induced changes of particle size and surface area was employed to model anthocyanin adsorption process numerically. Generally, sonication enhanced external mass transfer coefficient (k_L) and surface diffusion coefficient (D_s) during adsorption. The values of k_L and D_s under sonication at 279 W/L and 20 °C were 7.578×10^{-2} cm/s and 2.000×10^{-9} cm^2/s, which were 2.0% and 140.1% higher than the k_L and D_s values under orbital agitation at 20 °C. Accordingly, anthocyanins penetrated into the interior of macroporous resins faster under sonication. The overall intraparticle diffusion for anthocyanin adsorption was dominated by pore volume diffusion with the contribution percentage higher than 50%. Sonication enhanced the contribution of surface diffusion to the overall diffusion, which was consistent with the increase of D_s with ultrasound energy. Moreover, a general diffusion model also incorporating the variations of particle size and surface area was utilized to model anthocyanin desorption process. The overall anthocyanin diffusivity increased

* Corresponding author at: College of Food Science and Technology, Nanjing Agricultural University, Nanjing 210095, Jiangsu, China.
E-mail address: hanyongbin@njau.edu.cn (Y. Han).

https://doi.org/10.1016/j.cej.2019.122530
Received 10 June 2019; Received in revised form 14 August 2019; Accepted 16 August 2019
Available online 17 August 2019
1385-8947/ © 2019 Elsevier B.V. All rights reserved.

with both ultrasound energy level and temperature. Anthocyanins distributed more homogenously inside resins under sonication at 279 W/L than under other treatments. This work could be a reference for the valorization of anthocyanins in food industry, especially juice and wine industries.

Nomenclature

A	surface area (cm^2)
b	Langmuir constant (L/mg)
$C_{A,L}$	total anthocyanin concentration in liquid phase during adsorption (mg/L)
$C_{A,L,e}$	total anthocyanin concentration in liquid phase during adsorption at equilibrium (mg/L)
$C_{A,L,t}$	total anthocyanin concentration in liquid phase during adsorption at time t (mg/L)
$C_{A,L,0}$	initial concentration of total anthocyanins in liquid phase during adsorption (mg/L)
$C_{A,S}$	total anthocyanin concentration within macroporous resin during adsorption (mg/L)
$C_{D,L}$	total anthocyanin concentration in liquid phase during desorption (mg/L)
$C_{D,L,t}$	total anthocyanin concentration in liquid phase during desorption at time t (mg/L)
$C_{D,L,0}$	initial concentration of total anthocyanins in liquid phase during desorption (mg/L)
$C_{D,S}$	total anthocyanin concentration within macroporous resin during desorption (mg/L)
$C_{D,S,0}$	initial concentration of total anthocyanins within macroporous resin during desorption (mg/L)
D_{AB}	molecular diffusion coefficient of anthocyanins at infinite dilution (cm^2/s)
D_e	effective diffusion coefficient during desorption (cm^2/s)
D_{ep}	effective pore volume diffusion coefficient during adsorption (cm^2/s)
D_s	surface diffusion coefficient during adsorption (cm^2/s)
E	mean relative deviation modulus (%)
k_L	external mass transfer coefficient in liquid phase (cm/s)
m	mass of macroporous resins (g)
M_B	molecular weight of water (mol/g)
n	number of experimental data
$\boldsymbol{N}_{AP}$	mass flux due to pore volume diffusion (mg/cm^2 s)
$\boldsymbol{N}_{AS}$	mass flux due to surface diffusion (mg/cm^2 s)
PVSDM	pore volume and surface diffusion model
PVDCP	pore volume diffusion contribution percentage (%)
q_A	mass of anthocyanins adsorbed by macroporous resins (mg/g)
$q_{A,avg}$	mean value of mass of anthocyanins adsorbed by macroporous resin for all the experimental data (mg/g)
$q_{A,e}$	mass of anthocyanins adsorbed by macroporous resins at equilibrium (mg/g)
$q_{A,e,i}$	experimentally determined mass of anthocyanins adsorbed by macroporous resin (mg/g)
$q_{A,p,i}$	predicted mass of anthocyanins adsorbed by macroporous resin (mg/g)
q_D	mass of anthocyanins desorbed from macroporous resins (mg/g)
q_m	maximum adsorption capacity of macroporous resin predicted by Langmuir model (mg/g)
R	radius of macroporous resin (cm)
R^2	coefficient of determination
RMSE	root mean square error (mg/g)
S	external surface area per mass of macroporous resin (cm^2/g)
SDCP	surface diffusion contribution percentage (%)
t	time (min)
T	temperature (K)
V	volume of solution (mL)
V_A	molecular volume of anthocyanins (cm^3/mol)
V_L	volume of liquid phase during desorption (L)
X	radial distance (cm)

Greek symbols

τ	tortuosity factor of macroporous resin
ε_p	void fraction of macroporous resin
ρ_p	apparent density of macroporous resin (g/mL)
ρ_s	solid density of macroporous resin (g/mL)
φ	association factor of water (2.6)
η_B	viscosity of water at target temperature (cP)

1. Introduction

In the past decades, both academy and industry have put a lot of efforts into the recovery of polyphenols including anthocyanins from plant resources [1–3]. Due to the multiple bioactivities of polyphenols like antioxidant, anti-inflammatory, anti-microbial activities and others [4], the extraction and processing of plant polyphenols into commercial products is an important way for the utilization of plant materials. To obtain phenolics with considerably high purity from plant materials, the procedures about solvent extraction, purification, concentration and drying are usually needed [5]. Occasionally, encapsulation is also performed to enhance phenolic stability [6]. Throughout the entire processes, purification is a crucial procedure that directly determines the economic value of phenolic extract. The adsorption/desorption method using polymeric resins as adsorbent is a simple and attractive purification method [7,8]. However, the traditional adsorption/desorption procedure is usually time-consuming, and the recovery of phenolics is un-satisfactory [9,10]. Therefore, more efforts are needed to improve the purification of phenolics including anthocyanins by means of the adsorption/desorption method

Power ultrasound in the frequency range between 20 and 100 kHz is a versatile technology that has been widely applied in many processing areas, not limited to food processing [11,12]. In recent years, ultrasound has been more and more used in the adsorption and desorption treatments. Many studies have demonstrated that ultrasound can enhance various adsorption and desorption processes about pigments, metal ions and organic pollutants, owing to the mechanical and cavitational properties of ultrasound [9,13–15]. Our previous study also found that the incorporation of sonication into adsorption/desorption of blueberry anthocyanins on macroporous resins significantly improved the adsorption and desorption capacities, shortened the adsorption and desorption equilibrium time and enhanced the anthocyanin recovery [16]. Currently, most of the researches about ultrasound-assisted adsorption/desorption are focused on investigating the influence of ultrasound on the adsorption/desorption kinetics experimentally, modeling the kinetic data using simple models, and characterizing the adsorbent features analytically. Instead, the mechanism about ultrasonic enhancement of mass transfer during adsorption/desorption of phenolics including anthocyanins has been poorly studied.

Phenomenological modeling is an important way to explore the detailed mass transfer mechanism about adsorption and desorption

processes under investigation [17–19]. Generally, a series of mechanisms are involved in adsorption and desorption on porous materials. The influence of ultrasound on both adsorption and desorption mechanisms can be evaluated through using accurate mathematical expressions to describe the included mechanisms [20]. For this purpose, the diffusional theories coupled with numerical simulation can be employed to simulate adsorption/desorption processes, since both processes are dominated by the diffusion phenomenon [21–24]. In the case of phenomenological investigation of ultrasound-incorporated adsorption/desorption processes, Fröhlich et al. [25] modeled the mass transfer of ibuprofen adsorption on pre-sonicated activated carbon numerically and explored the influence of ultrasound pretreatment on the subsequent adsorption behavior. Meanwhile, Ondarts et al. [26] studied the ibuprofen adsorption on activated carbon in the presence of ultrasound irradiation by diffusional modeling. Other studies about mass transfer investigation of ultrasound-related adsorption/desorption have been rarely reported. On the other hand, it has been widely recognized that ultrasound cavitation can change the adsorbent properties, especially the particle size [15,27]. In this case, both the mass transfer distance and surface area relating to mass transfer are changeable during sonication. According to our best knowledge, the current diffusional models have not yet considered the changes of particle size and surface area of adsorbent for the simulation of ultrasound-enhanced adsorption/desorption processes.

Our previous study studied the influence of ultrasound on the adsorption and desorption kinetics of blueberry anthocyanins using macroporous resins as adsorbent experimentally [16]. However, the detailed mass transfer mechanisms about the adsorption/desorption processes under sonication were still unknown. Following the previous work, the detailed mass transfer mechanism about ultrasound enhanced adsorption and desorption on macroporous resins were explored by diffusional modeling numerically in this work. The changes of resin properties during sonication, including average pore diameter, specific surface area, total pore volume and particle size were monitored. Then, a pore volume and surface diffusion model incorporating the changes of resin properties (particle size and surface area) was employed to simulate the ultrasound-enhanced adsorption process. The contribution of each diffusion mechanism in the overall mass transfer mechanism was also analyzed. Moreover, a general diffusion model with the variation of resin properties was utilized to simulate the desorption process. Besides, anthocyanin adsorption/desorption processes were visualized following mass transfer modeling results.

2. Materials and methods

2.1. Materials

Crude anthocyanin extract was obtained by solvent extraction from fresh blueberries, using distilled water containing 0.02% hydrochloric acid as solvent. Macroporous resins (XAD-7HP) were activated by sequential 95% ethanol elution, deionized water elution, 4% hydrochloric acid elution, deionized water elution, 5% sodium hydroxide elution and deionized water elution. The details about anthocyanin extraction and resin preparation were well described in our previous study [16].

2.2. Ultrasound-assisted adsorption and desorption kinetics

The experimental procedures about ultrasound-assisted adsorption and desorption were also well depicted in our previous study [16]. Briefly, the adsorption and desorption experiments with the assistance of sonication were performed in a thermostatic water bath equipped with an impeller (DC-0506, Fandilang Tech, Nanjing, China).

For adsorption treatment, 0.5 g activated resins and 50 mL crude anthocyanin extract were mixed together in a 100-mL Erlemeyer flask. This flask was then moved to a water bath system and an ultrasonic probe (20 kHz in frequency and 1 cm in diameter) was inserted into the dispersion. The total anthocyanin content in the solution was analyzed periodically using the spectrometric method described by Ivanova et al. [28]. For desorption treatment, macroporous resins were immersed in blueberry anthocyaninic solutions at 20 °C and orbital agitation for 24 h. Then, 0.5 g intact macroporous resins loaded with blueberry anthocyanins were mixed with 50 mL 80% aqueous ethanol in a 100-mL Erlemeyer flask. This flask was then placed in the water bath system and the same ultrasound probe was inserted inside. The total anthocyanin concentration in the solution was determined periodically.

Both adsorption and desorption processes were performed at acoustic energy density (AED) levels of 106, 199 and 279 W/L, and temperature levels of 20 and 30 °C, respectively. Sonication was conducted at a pulsed mode (5 s on, 5 s off). All the experiments were replicated three times.

The adsorption and desorption capacities of anthocyanins were calculated as:

$$q_A = \frac{(C_{A,L,0} - C_{A,L,t})}{m} V \tag{1}$$

$$q_D = \frac{(C_{D,L,t} - C_{D,L,0})}{m} V \tag{2}$$

2.3. Determination of adsorption isotherm

The experimental procedures for isotherm study were similar to the adsorption test described in Section 2.2. Briefly, blueberry anthocyanin extracts with the concentrations of 50, 100, 150, 200 and 250 mg/L were prepared through dilution and vacuum concentration. Then, 0.5 g macroporous resins and 50 mL anthocyanin extract were blended at different temperatures (20 and 30 °C) and AED (106, 199 and 279 W/L) levels, respectively. Sonication lasted for 5 h, so as to ensure the achievement of adsorption equilibrium. Total anthocyanin concentration was then determined and the amount of anthocyanin adsorbed was calculated. For the comparison purpose, the adsorption isotherms under orbital vibration at 100 rpm were also established.

To build a quantitative relationship between the amount of anthocyanins adsorbed by macroporous resins and the amount of anthocyanins in liquid phase, the experimental data were fitted to the widely used Langmuir isotherm model [25]:

$$q_{A,e} = \frac{q_m b C_{A,L,e}}{1 + b C_{A,L,e}} \tag{3}$$

2.4. Characterization of macroporous resin under sonication

The parameters about particle size and porosity of macroporous particle that needed to be considered for simulation were analyzed. For this purpose, the particle size distribution of macroporous resin samples during ultrasound-assisted adsorption was measured in a Malvern MAZ3000 laser diffraction particle size analyzer (Malvern Instruments, UK). The specific surface area and pore size of resin particle, which can reflect resin porosity [15], were assessed by N_2 adsorption method in a BELSORP-mini adsorption apparatus (Bel Japan Inc, Japan).

The solid density (ρ_p) of macroporous resin particles was measured by the picnometry method, while the apparent density was measured from the values of solid density and pore volume [25]. The void fraction (ε_p) of macroporpous resin was estimated using the following equation [29]:

$$\varepsilon_p = 1 - \frac{\rho_p}{\rho_s} \tag{4}$$

The obtained ε_p value was 0.339. For the comparison purpose, the aforementioned resin properties were also monitored during orbital agitation.

2.5. Mass transfer modeling

2.5.1. Adsorption modeling

The diffusional model considering external mass transfer referring to anthocyanin penetration through liquid film surrounding macroporous resins, intraparticle diffusion and adsorption on active sites at pore surface was employed to simulate the adsorption process [21,30]. For intraparticle diffusion, the diffusion in the pore volume of macroporous resins and surface diffusion were taken into consideration simultaneously [25]. Thus, the diffusional model is usually named as pore volume and surface diffusion model (*PVSDM*). Moreover, macroporous resins were assumed to be spherical and isotropic, and the suspension was perfected mixed due to the ultrasound-induced agitation or orbital vibration. Bearing the aforementioned factors in mind, the governing equation describing mass balance into a resin particle is written as:

$$\varepsilon_p \frac{\partial C_{A,S}}{\partial t} + \rho_p \frac{\partial q_A}{\partial t} = \frac{1}{x^2}\frac{\partial}{\partial x}\left(x^2\left(D_{ep}\frac{\partial C_{A,S}}{\partial x} + D_s\rho_p\frac{\partial q_A}{\partial x}\right)\right) \tag{5}$$

The initial conditions for Eq. (5) are defined as:

$$t = 0 \quad C_{A,L} = C_{A,L,0} \quad C_{A,S} = 0 \quad q_A = 0 \tag{6}$$

The boundary conditions are expressed as:

$$\left.\frac{\partial C_{A,S}}{\partial x}\right|_{x=0} = 0 \tag{7}$$

$$D_{ep}\left.\frac{\partial C_{A,S}}{\partial x}\right|_{x=R} + D_s\rho_p\left.\frac{\partial q_A}{\partial x}\right|_{x=R} = k_L(C_{A,L} - C_{A,S}) \tag{8}$$

Two independent variables, namely $C_{A,S}$ and q_A, were included in the *PVSDM* model. A quantitative relationship between $C_{A,S}$ and q_A can be built by the adsorption isotherm model represented by Eq. (3), since the adsorption rate on active sites was usually instantaneous and consequently local equilibrium on solid-liquid interface can be achieved [31]. The term $C_{A,S}$ can be substituted by q_A in the *PVSDM* model, thus reducing the number of independent variables. Consequently, the governing equation and initial and boundary conditions of the *PVSDM* model can be transformed to:

$$\left(\varepsilon_p\frac{q_m b}{(q_m b - bq_A)^2} + \rho_p\right)\frac{\partial q_A}{\partial t} = \frac{1}{x^2}\frac{\partial}{\partial x}\left(x^2\left(D_{ep}\frac{q_m b}{(q_m b - bq_A)^2} + D_S\rho_p\right)\frac{\partial q_A}{\partial x}\right) \tag{9}$$

$$t = 0 \quad q_A = 0 \tag{10}$$

$$\left.\frac{q_m b}{(q_m b - bq_A)^2}\frac{\partial q_A}{\partial x}\right|_{x=0} = 0 \tag{11}$$

$$D_{ep}\left.\frac{q_m b}{(q_m b - bq_A)^2}\frac{\partial q_A}{\partial x}\right|_{x=R} + D_s\rho_p\left.\frac{\partial q_A}{\partial x}\right|_{x=0} = k_L(C_{A,L} - C_{A,S}) \tag{12}$$

Before solving the *PVSDM* model, the parameters k_L, D_{ep} and D_s needed to be estimated. The values of k_L can be estimated from Eq. (13) proposed by Furusawa and Smith [32], which was widely used in well-agitated systems:

$$\left(\frac{d\left(\frac{C_{A,L}}{C_{A,L,0}}\right)}{dt}\right)_{t\to 0} = -\frac{mSk_L}{V} \tag{13}$$

The data about $C_{A,L}$ at $t = 0$ min and $t = 10$ min were used for calculation and the k_L value was obtained from the slope of total anthocyanin concentration decay. Herein, the value of surface area S was considered to be constant within a short sonication duration, which was calculated as [21]:

$$S = \frac{3}{R\rho_p} \tag{14}$$

The D_{ep} values were determined using the following equation [25]:

$$D_{ep} = \frac{\varepsilon_p}{\tau}D_{AB} \tag{15}$$

According to the studies of Adamíková et al. [33], Komiyama and Smith [34] and Monsanto et al. [35], the τ value was considered to be 1.4, which was a typical value for commercial macroporous resins. This value also located in the tortuosity range of many porous particles reported by Barrande et al. [36]. Meanwhile, the D_{AB} value of anthocyanins was calculated using the method of Wilke and Chang [37]:

$$D_{AB} = 7.4 \times 10^{-8}\frac{T(\varphi M_B)^{0.5}}{\eta_B V_A^{0.6}} \tag{16}$$

Among the involved parameters in Eq. (16), the association factor φ for water was 2.6 [38]. The viscosities of water at 20 and 30 °C were 1.0050 and 0.8007 cP, respectively. The molecular diffusion coefficient of red grape anthocyanins (7.86×10^{-10} m^2/s) in methanol at 40 °C reported by Mantell et al. [39] was employed as a reference to calculate the D_{AB} values of anthocyanins in water.

Another important issue that should be addressed was the ultrasonic-induced disruption of resin particles, making the moving distance of anthocyanins and surface area relating to anthocyanin exchange changeable during sonication [16]. Thus, the ultrasound-assisted adsorption process was featured as a moving boundary problem. To incorporate the factor of variations of particle size and surface area into *PVSDM* model easily, resin particles were assumed to maintain their spherical geometry during sonication. The quantitative pattern about particle size change built in Section 2.4 was then used to calculate the radius and surface area of macroporous resin at each sampling time.

Once the values of k_L, D_{ep}, resin radius and surface area at different periods of adsorption were obtained, the *pdepe* function in Matlab (R2010a, The MathWorks, Inc., MA, USA) was used to solve the *PVSDM* model numerically. The D_s value was changed iteratively to fit the experimental data until the *RMSE* value between experimental and predicted results reached the minimum:

$$RMSE = \sqrt{\frac{1}{n}\sum_{i=1}^{n}(q_{A,e,i} - q_{A,p,i})^2} \tag{17}$$

After the optimization of D_s value, another two statistical indicators R^2 and E (%) were calculated to further test the predictive accuracy of *PVSDM* model:

$$R^2 = 1 - \frac{\sum_{i=1}^{n}(q_{A,e,i} - q_{A,p,i})^2}{\sum_{i=1}^{n}(q_{A,e,i} - q_{A,avg})^2} \tag{18}$$

$$E(\%) = \left(\frac{\sum_{i=1}^{n}|q_{A,e,i} - q_{A,p,i}|/q_{A,e,i}}{n}\right) \times 100 \tag{19}$$

Moreover, the numerical results were coded in Matlab to visualize the changes of anthocyanin content within macroporous resins during adsorption.

2.5.2. Desorption modeling

The desorption process can be depicted as the movement of anthocyanins from macroporous resins to the elution solvent, which was similar to the traditional solid-liquid extraction process [40]. Thus, the transport of anthocyanins within resin particles can also be regarded as a diffusion phenomenon. To simplify the modeling task, macroporous resins were considered as intact particles and the porosity factor was temporarily ignored. In many papers about solid-liquid extraction of target compounds from porous materials, the porosity property was also excluded from the model [40–42]. Moreover, several assumptions were also made, including the spherical geometry of resin particles,

homogenous distribution of anthocyanins inside macroporous resins before desorption, constant D_e values of anthocyanins during desorption and perfect mixing of the suspension. Then, the diffusional model for spherical geometric shape can be used to simulate the desorption process [41]:

$$\frac{\partial C_{D,S}}{\partial t} = D_e\left(\frac{1}{x^2}\frac{\partial}{\partial x}\left(x^2\frac{\partial C_{D,S}}{\partial x}\right)\right) \tag{20}$$

The initial conditions for Eq. (20) are:

$$t = 0 \quad C_{D,S} = C_{D,S,0} \quad C_{D,L} = 0 \tag{21}$$

The boundary conditions for Eq. (21) are:

$$\left.\frac{\partial C_{D,S}}{\partial x}\right|_{x=0} = 0 \tag{22}$$

$$D_e A\left.\frac{\partial C_{D,S}}{\partial x}\right|_{x=R} = V_L\frac{dC_{D,L}}{dt} \tag{23}$$

Eq. (23) described the equality relationship between the outcoming flux of anthocyanins from macroporous resins during desorption and the incoming flux in the elution solvent [43]. Similar to the adsorption process, the desorption process still belonged to a moving boundary

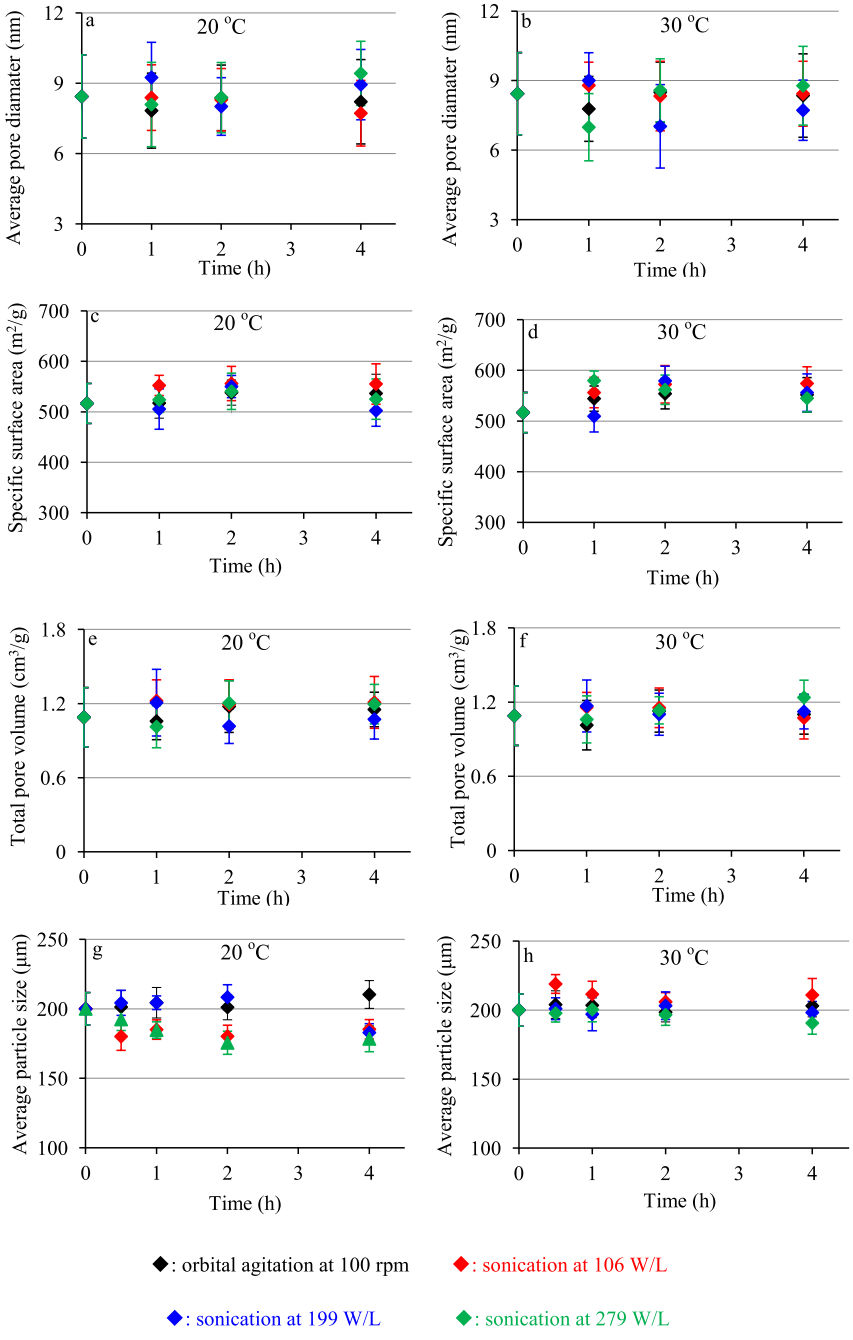

Fig. 1. Changes of average pore diameter (a and b), specific surface area (c and d), total pore volume (e and f) and average particle size (g and h) of macroporous resins under orbital agitation and sonication.

problem due to the ultrasound-induced disruption of resin particles. Thus, the pattern about particle size variation in ultrasonic fields mentioned in Section 2.4 was also used to calculate the radius values and surface area of macroporous resins during desorption. The desorption model was solved by "*pdepe*" function in Matlab. The D_e value was optimized to obtain the minimal value of *RMSE* value between experimental and predicted desorption capacity. Then, R^2 and E (%) values were also calculated to validate the desorption model. Finally, the variations of anthocyanin content within macroporous resins during desorption were visualized using numerical simulation results through programming coding in Matlab.

3. Results and discussion

3.1. Characterization of macroporous resin under sonication

The N_2-BET method was used to determine the textural properties of macroporous resin at different periods of sonication. The variations of average pore diameter, specific surface area and total pore volume as a function of treatment time are plotted in Fig. 1(a–f). The average pore diameter, specific surface area and total pore volume of macroporous resin before adsorption are 8.432 ± 1.774 nm, 516.5 ± 39.7 m^2/g and 1.089 ± 0.240 cm^3/g, respectively. Neither sonication nor orbital agitation resulted in marked changes of these resin properties. These results were similar to the findings reported by Ondarts et al. [26], who found that the texture of activated carbon fabric remained unchanged in the case of ibuprofen adsorption assisted by 20-kHz sonication. On the contrary, the studies of Fröhlich et al. [25] and Low et al. [15] found that ultrasound treatment increased the surface area, pore volume and pore size of vegetable activated carbon and peanut husk powder, thus creating more pores, exposing more binding sites and improving the subsequent adsorption processes. It is reasonable that biological adsorbents are more liable to be affected by ultrasound than polymeric materials, because biological adsorbents normally have softer textures. Moreover, the insignificant influence of ultrasound on macroporous resin texture may also be related to the low values of pore diameter. According to the literature, the size of ultrasound cavitation bubbles usually locates in the micrometer scale [44,45], while the pore diameter of macroporous resin XAD-7HP was approximately 8 nm. In this circumstance, cavitation bubbles could not easily penetrate into the interior of macroporus resin to modify resin texture.

On the other hand, the size of resin particles exhibited a decreasing trend in ultrasonic field, whereas no clear influence of orbital agitation on resin size was observed (Fig. 1g and h). Here, the initial average particle size of macroporous resin was 200.1 ± 11.7 μm. After 4-h sonication at 20 °C, the average particle size of resins treated by orbital agitation and sonication at 106, 199 and 279 W/L were 210.3 ± 10.6, 185.2 ± 7.8, 182.9 ± 6.4 and 178.4 ± 9.3 μm, respectively. In the meantime, macroporous resins sonicated at 30 °C were featured by larger particle size than resins sonicated at 20 °C. For example, after sonication at 279 W/L for 4 h, the average particle sizes of macroporous resins treated at 20 and 30 °C were 178.4 ± 9.3 and 190.6 ± 8.1 μm, respectively. Temperature rising could promote the swelling of macroporous resins [46], as well as weaken the energy produced by collapse of ultrasound cavitation bubbles [47]. As a result, sonication at 20 °C had a profounder influence on the size of resin particles. Since no evident pattern about the decrease of resin particle size was observed in Fig. 1g and h, it was tentatively assumed that macroporous resins still can maintain their spherical geometry under sonication, while their diameter value decreased linearly [16,48]. This assumption was used to calculate resin size and surface area at each sampling time during both adsorption and desorption processes, when solving the diffusional models numerically.

3.2. Adsorption isotherm under sonication

The equilibrium isotherms for anthocyanin adsorption on macroporous resins under sonication at 20 and 30 °C are illustrated in Fig. 2. As can be seen, the adsorption isotherm data for ultrasound-assisted adsorption always located above the adsorption data under orbital vibration. This result was consistent with the kinetic results published previously [16], corroborating that ultrasound can promote the attachment of anthocyanins on macroporous resins in the current experimental range. The experimental data were fitted to the Langmuir isotherm model with acceptable accuracies (Fig. 2 and Table 1). Interestingly, the amount of anthocyanins adsorbed appeared to approach a limited value with the increase of total anthocyanin concentration at equilibrium under sonication at 199 and 279 W/L, whereas the adsorption capacities increased continuously under sonication at 106 W/L and orbital agitation within the applied anthocyanin equilibrium concentrations. The maximum adsorption capacity derived from Langmuir isotherm model also decreased with the increase of AED level. It was tentatively speculated that extremely high ultrasound energies may decrease the stability of anthocyanins in liquid, thus hindering the binding between anthocyanins and macroporous resins [49]. Moreover, the destructive effect of ultrasound, especially at very high energy levels, may destroy the available surface area of macroporous resins,

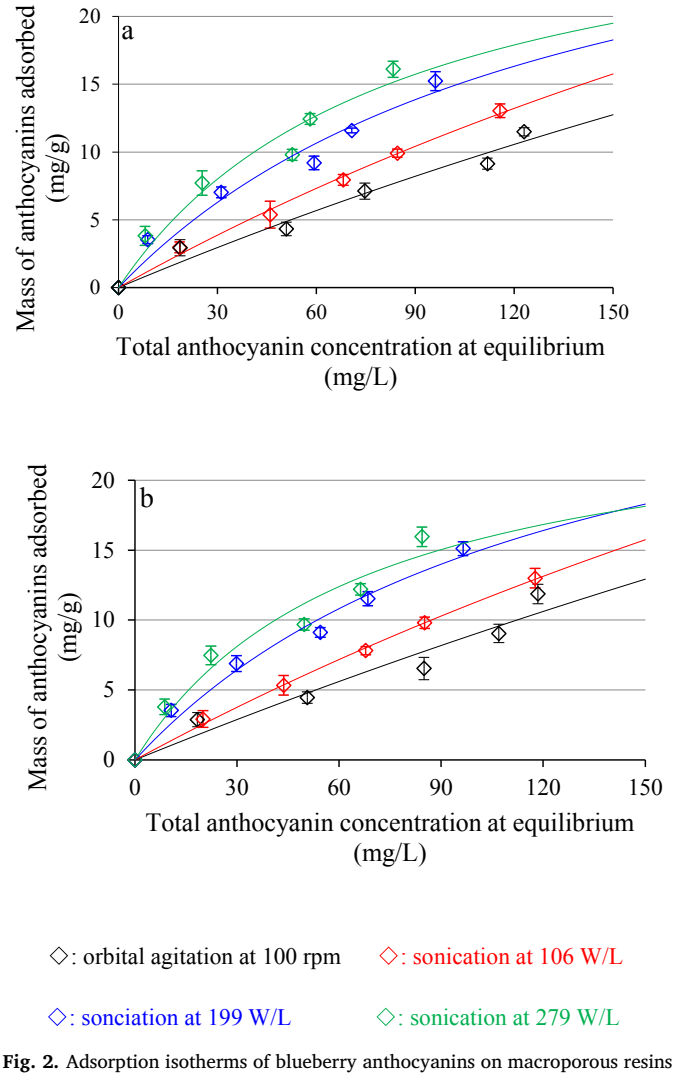

Fig. 2. Adsorption isotherms of blueberry anthocyanins on macroporous resins at 20 °C (a) and 30 °C (b). The lines denote the Langmuir isotherms.

Table 1
Constants of Langmuir isotherms for blueberry anthocyanin adsorption on macroporous resins.

Temperature	Condition	q_m (mg/g)	$b \times 10^3$ (L/mg)	R^2	*RMSE*
20 °C	Orbital agitation	74.9	1.369	0.971	0.808
	Sonication at 106 W/L	68.3	2.001	0.995	0.322
	Sonication at 199 W/L	34.9	7.316	0.967	1.109
	Sonication at 279 W/L	30.4	11.890	0.962	1.270
30 °C	Orbital agitation	99.1	1.001	0.946	0.995
	Sonication at 106 W/L	76.9	1.717	0.998	0.217
	Sonication at 199 W/L	33.9	7.800	0.966	1.289
	Sonication at 279 W/L	26.2	14.930	0.937	1.973

which could also weaken the adsorption capacity of macroporous resins. This quantitative relationship between $q_{a,e}$ and $C_{A,L,e}$ defined by Langmuir isotherm model was then used in the *PVSDM* model, so as to clarify the mechanism for ultrasound-enhanced adsorption of blueberry anthocyanins on macroporous resins.

3.3. Numerical simulation of adsorption process under sonication

The *PVSDM* model considering both pore volume and surface diffusions was utilized to interpret anthocyanin transfer within macroporous resins during adsorption. For pore volume diffusion, the driving force was the anthocyanin concentration gradient in the liquid within resin pores, while the driving force for surface diffusion was the mass uptake gradient on adsorbents [21].

Prior to solving the *PVSDM* model numerically, the mass transfer parameters including k_L, D_{AB} and D_{ep} at 20 and 30 °C were calculated and given in Table 2. In the studied experimental conditions, k_L values ranged from 7.419×10^{-2} to 7.578×10^{-2} cm/s. At both temperatures, the external mass transfer coefficient under sonication at 106 W/L was close to the k_L values under orbital agitation. Meanwhile, the k_L value increased with the increase of input ultrasound energy. These results were consistent with our previous study in the case of ultrasound-assisted biosorption of phenolics on yeasts [27]. At the same AED level, the k_L value at 20 °C was always slightly higher than that at 30 °C. This phenomenon can be attributed to the negative effect of temperature on the energies released by the collapse of ultrasound cavitation bubbles. Temperature rising attenuated the ultrasound cavitation energy [47], thus lowering the ultrasonic intensification of external mass transport during adsorption.

The D_{AB} values of anthocyanins in water at 20 and 30 °C were 2.818×10^{-6} and 3.658×10^{-6} cm^2/s, which were calculated on the basis of the corresponding value of anthocyanins in methanol reported by Mantell et al. [39]. Using these D_{AB} values for another calculation shown in Eq. (15), the D_{ep} values for anthocyanins were estimated to be 6.820×10^{-7} m^2/s at 20 °C and 8.860×10^{-7} m^2/s at 30 °C. Temperature increase can enhance the pore diffusivity of anthocyanins, which was consistent with the study of Tao et al. [50] in the case of identifying phenolic diffusivity during ultrasound extraction. The pore diffusion coefficients for anthocyanins in macroporous resins at 20 and 30 °C were close to that for ibuprofen in activated carbon at 25 °C [25],

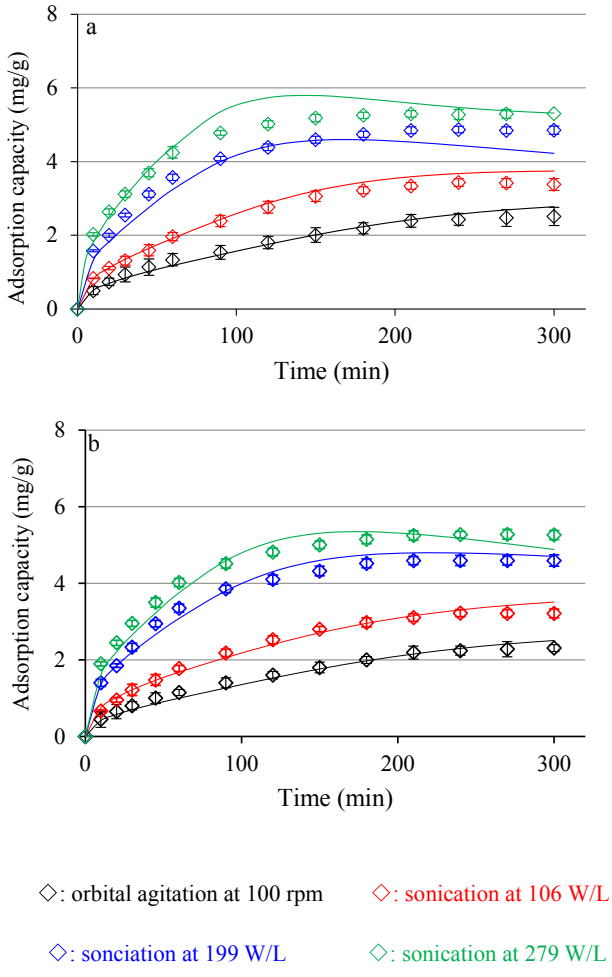

Fig. 3. Experimental versus predicted amounts of anthocyanins adsorbed on macroporous resins at 20 °C (a) and 30 °C (b). Solid line: diffusional modeling results. Experimental data about ultrasound-assisted adsorption were taken from Wu et al. [16].

Table 2
Mass transfer parameters about anthocyanin adsorption on macroporous resins and accuracy of the *PVSDM* model.

Temperature	Condition	$k_L \times 10^2$ (cm/s)	$D_{AB} \times 10^6$ (cm^2/s)	$D_{ep} \times 10^7$ (cm^2/s)	$D_S \times 10^9$ (cm^2/s)	R^2	*RMSE* (mg/g)	*E* (%)
20 °C	Orbital agitation	7.433	2.818	6.820	0.833	0.984	0.118	5.416
	Sonication at 106 W/L	7.444			1.167	0.997	0.175	4.441
	Sonication at 199 W/L	7.524			1.833	0.984	0.317	7.311
	Sonication at 279 W/L	7.578			2.000	0.983	0.345	5.773
30 °C	Orbital agitation	7.422	3.658	8.860	0.850	0.988	0.103	6.782
	Sonication at 106 W/L	7.419			0.917	0.989	0.120	4.337
	Sonication at 199 W/L	7.512			1.500	0.990	0.181	4.211
	Sonication at 279 W/L	7.564			1.667	0.982	0.239	5.756

but lower than the values for phenolics in Sephabeads SP206 polymeric resins between 20 and 60 °C [38]. Generally, a variety of factors can influence the pore diffusivity of adsorbate according to Eqs. (15) and (16).

Using the aforementioned k_L and D_{ep} values, the *PVSDM* model was solved and the obtained D_s values are listed in Table 2. In the meantime, the predicted adsorption capacities were compared with the experimental data in Fig. 3. As can be seen, the *PVSDM* model was qualified to predict the adsorption capacity of anthocyanins on macroporous resins under sonication, although there were some divergences between experimental and predicted values at certain points. In Table 2, the R^2 values at all the tested conditions exceeded 0.98, and E (%) values were lower than 10%. These statistical results also implied that *PVSDM* model was reliable to simulate the adsorption process. Similar to the influence of ultrasound on external mass transfer, the D_s values also increased along with the increase of AED level. Using adsorption at 20 °C for example, the D_s value under orbital agitation was 0.833×10^{-9} cm^2/s and the D_s value under sonication at 279 W/L increased to 2.000×10^{-9} cm^2/s. The D_s value under sonication at 279 W/L and 30 °C was also 96.1% higher than the D_s value under orbital agitation at the same temperature. Taking the influences of ultrasound on both k_L and D_s into account, it can be concluded that

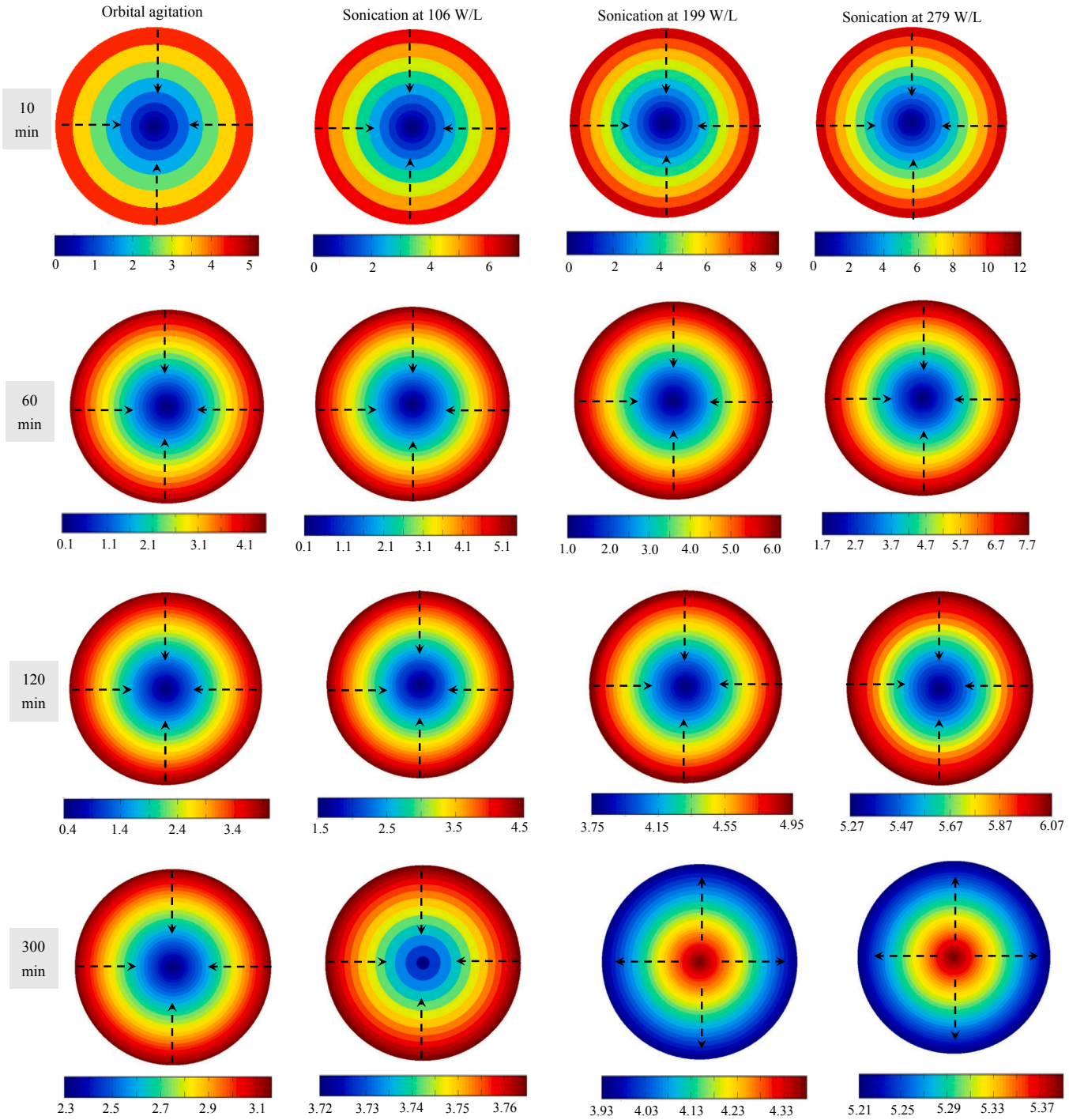

Fig. 4. Distribution of mass of anthocyanins adsorbed (mg/g) along with the radial direction of macroporous resins during adsorption at 20 °C. The arrow refers to the mass transfer direction.

ultrasound enhanced both external film penetration and interior mass uptake on solid phase to accelerate the anthocyanin adsorption process.

Following the numerical results, the distributions of mass of anthocyanins adsorbed q_A and total anthocyanin concentration in the liquid phase $C_{A,S}$ along with the radial direction of macroporous resins during adsorption at 20 °C are visualized in Fig. 4 and Supplementary Fig. 1. It can be seen that there were high mass uptake gradient and anthocyanin concentration gradient within macroporous resins at the early stage of adsorption. Along with the increase of adsorption time, both anthocyanin mass and concentration gradients got attenuated. After adsorption for 300 min, the mass transfer direction under orbital agitation and sonication at 106 W/L remained towards the core of resin particles. Instead, the anthocyanin movement pathway under sonication at 199 and 279 W/L was from the core to the exterior, due to the slightly higher anthocyanin concentration and mass uptake in the center of macroporous resins.

To estimate the contributions of pore volume diffusion and surface diffusion to the overall intraparticle diffusion of anthocyanins, the mass fluxes due to pore volume diffusion ($\boldsymbol{N}_{AP}$) and surface diffusion ($\boldsymbol{N}_{AS}$) were calculated as follows:

$$\boldsymbol{N}_{AP} = -D_{ep}\frac{\partial C_{A,S}}{\partial x} \tag{24}$$

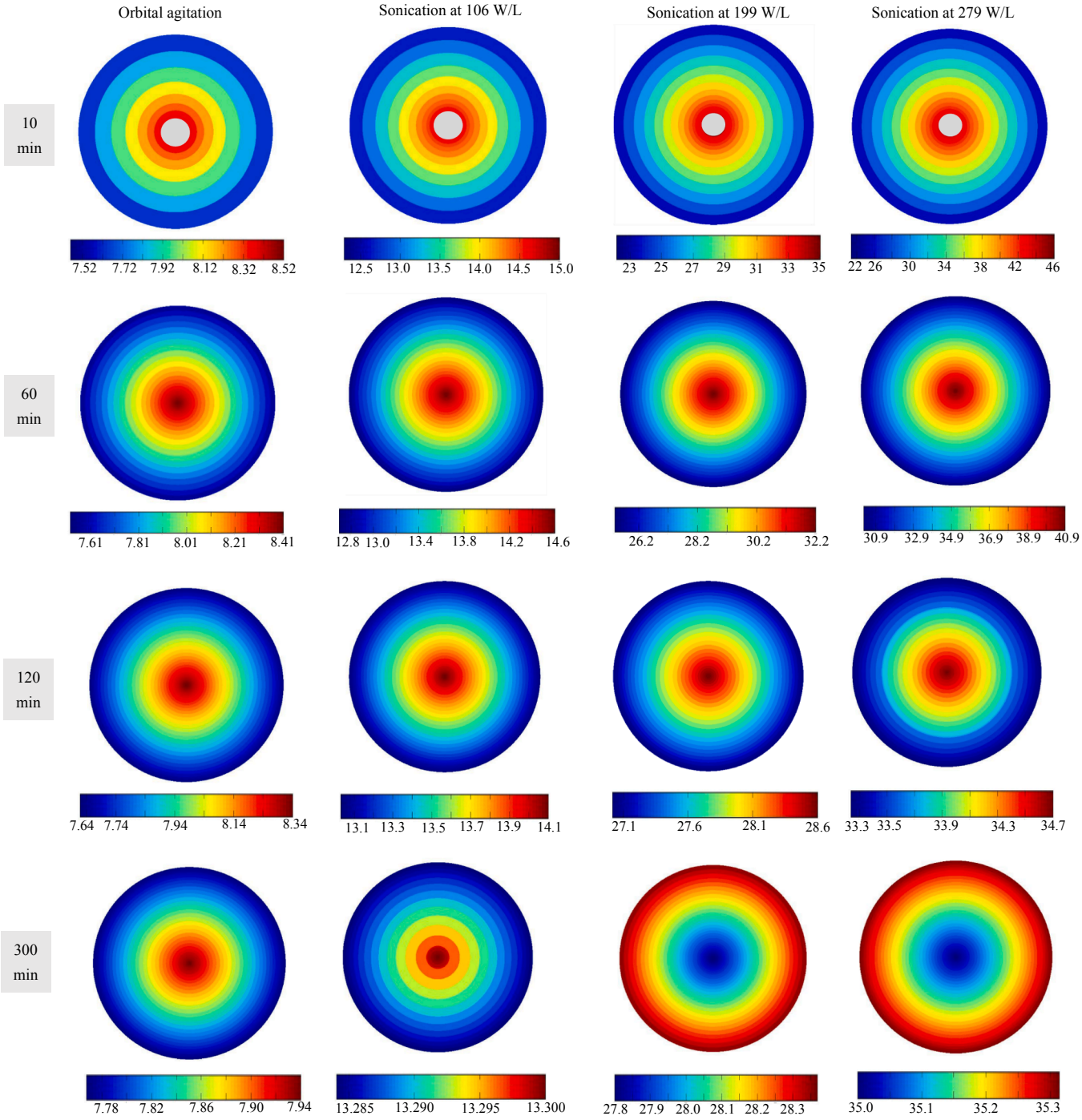

Fig. 5. Changes of surface diffusion contribution percentage (*SDCP*%) along with the radial direction of macroporous resins during adsorption at 20 °C. The gray area means no diffusion area.

$$\boldsymbol{N}_{AS} = -D_S \rho_p \frac{\partial q_A}{\partial x} \quad (25)$$

The resulting magnitude and direction of $\boldsymbol{N}_{AP}$ and $\boldsymbol{N}_{AS}$ during adsorption at 20 °C are illustrated in Supplementary Figs. 2 and 3. The surface diffusion contribution percentage (*SDCP*%) was then calculated using the following equation on the basis of resulting $\boldsymbol{N}_{AP}$ and $\boldsymbol{N}_{AS}$ values [21]:

$$SDCP\% = \frac{\|\boldsymbol{N}_{AS}\|}{\|\boldsymbol{N}_{AS}\| + \|\boldsymbol{N}_{AP}\|} \times 100 \quad (26)$$

The variations of *SDCP*% during anthocyanin adsorption on macroporous resins at 20 °C are plotted in Fig. 5. Generally, the *SDCP*% value for the investigated adsorption processes ranged from 7% to 45%, indicating that pore volume diffusion contributed more than surface diffusion to the overall intraparticle diffusion of anthocyanins. On the contrary, Díaz-Blancas et al. [21], Fröhlich et al. [25] and Ocampo-Perez et al. [23] all found that surface diffusion played a dominant role in the whole intraparticle diffusion in the cases of metronidazole, ibuprofen and pyridine adsorptions onto activated carbon. The differences in *SDCP*% between the current results and literature reports were probably due to the diversity of adsorbent properties, since a variety of adsorbent properties including porosity, density, size and tortuosity can affect the diffusion process.

According to Fig. 5, there was no diffusion phenomenon occurred in the core area of marcoporous resins at the beginning of adsorption. After adsorption for 10 min, the grey area referring to no diffusion decreased with the increase of applied ultrasound energy, further demonstrating that sonication promote the penetration of anthocyanins into the interior of macroporous resins. Meanwhile, ultrasound treatment enhanced the contribution of surface diffusion to the overall diffusion. For adsorption under orbital agitation, the *SDCP*% value changed between 7.0% and 8.5% throughout the whole adsorption process. Instead, the highest and lowest *SDCP*% values increased to 44.0% and 23.0% for ultrasound-assisted adsorption at 279 W/L, both of which were obtained after 10-min sonication. For adsorption with the assistance of ultrasound, there was a high gradient of *SDCP*% within resin particles at the early stage of adsorption. The *SDCP*% value decreased along with the radical direction. With the increase of adsorption time, the *SDCP*% value distributed more homogeneously inside ultrasound-treated macroporous resins, which was consistent with the changes of q_A and $C_{A,s}$ exhibited in Fig. 4 and Supplementary Fig. 1.

Through the aforementioned illustration, the mass transfer pathway of anthocyanins under adsorption with and without sonication was clearly explained. The modeling results also demonstrated that both surface diffusion and pore volume diffusion mechanisms occurred simultaneously.

3.4. Numerical simulation of desorption process under sonication

The anthocyanin desorption process with the assistance of ultrasound was simulated by the general diffusional model considering the influence of ultrasound on resin size successfully (Fig. 6). The statistical analysis results exhibited in Table 3 showed that the diffusional model was characterized by low E % values (lower than 3%) and high R^2 values (approaching 1), implying the high predictive accuracy of the diffusional model. The D_e values in the selected desorption conditions ranged from 1.667×10^{-5} to 5.833×10^{-5} cm^2/s, all of which were two orders of magnitudes higher than the D_{ep} values and four orders of magnitudes higher than D_s values during adsorption. The higher diffusivity of anthocyanins during desorption was consistent of the shorter time required to reach the equilibrium. All the desorption process reached the equilibrium within 1 h (Fig. 6), whereas it took approximately 3 h for the adsorption to reach the equilibrium (Fig. 3). Moreover, the D_e values during anthocyanin desorption were markedly higher than the corresponding D_e values for total phenolics in the cases of phenolic extraction from grape stalks, chokeberry powders and roselle calyces [40,41,50]. It was deduced that the higher porosity of maroporous resins made the diffusion of anthocyanins within resin particles easier than that within plant materials.

The diffusion coefficient of anthocyanins increased with the increase of AED level and temperature. For example, the D_e value during desorption under sonication at 279 W/L and 20 °C was 5.333×10^{-5} cm^2/s, which was 220.0% higher than the D_e values (1.667×10^{-5} cm^2/s) under orbital agitation at 20 °C. Meanwhile, the D_e value (5.833×10^{-5} cm^2/s) during ultrasound-enhanced desorption at 279 W/L and 30 °C was 9.4% higher than the corresponding D_e value at 20 °C. Similar results were found in many papers about ultrasound-assisted extraction [50,51]. On one hand, the presence of ultrasound cavitation can facilitate the movement of anthocyanins within macroporous resins undoubtedly. On the other hand, temperature rising enhanced the mobility and internal energy of anthocyanin molecules, as well as lowered the dynamic viscosity coefficient of elution solvent [40]. Consequently, the effective diffusivity of anthocyanins increased with temperature during desorption. The influence of temperature on anthocyanin diffusivity during desorption was different from that during adsorption (Tables 2 and 3), indicating that there existed some differences in mass transfer mechanisms between anthocyanin adsorption and desorption.

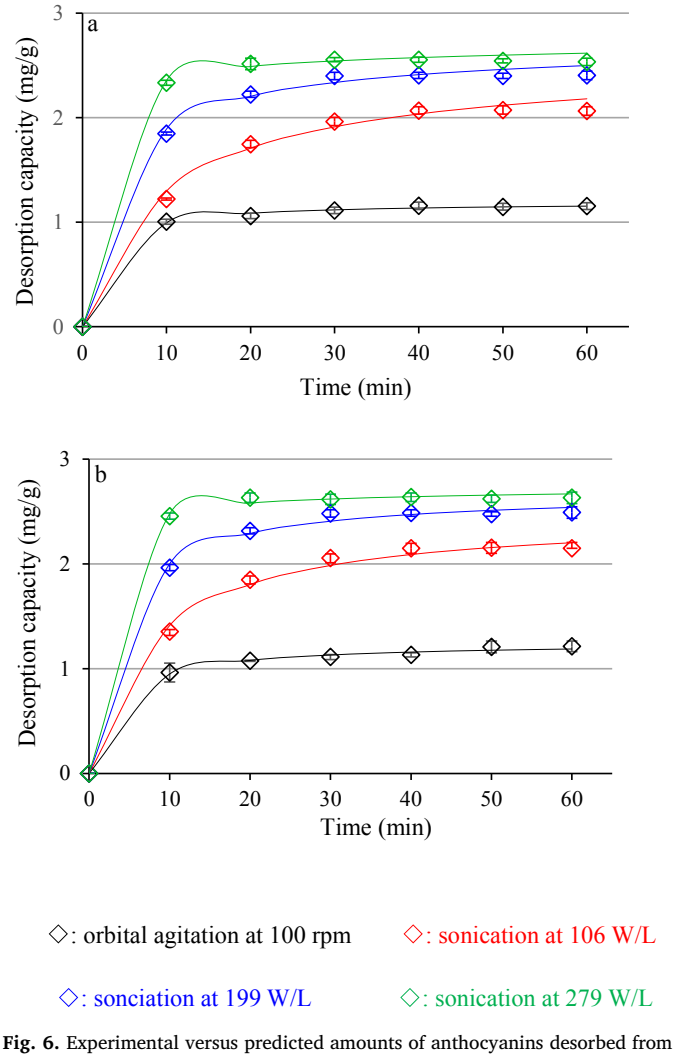

Fig. 6. Experimental versus predicted amounts of anthocyanins desorbed from macroporous resins at 20 °C (a) and 30 °C (b). Solid line: diffusional modeling results. Experimental data about ultrasound-assisted desorption were taken from Wu et al. [16].

Table 3
Mass transfer parameters about anthocyanin desorption from macroporous resins and accuracy of the general diffusional model.

Temperature	Condition	$D_e \times 10^5$ (cm^2/s)	R^2	*RMSE* (mg/g)	*E* (%)
20 °C	Orbital agitation	1.667	0.999	0.013	0.852
	Sonication at 106 W/L	2.500	0.993	0.062	2.936
	Sonication at 199 W/L	4.167	0.997	0.053	1.834
	Sonication at 279 W/L	5.333	0.999	0.041	1.234
30 °C	Orbital agitation	2.500	0.997	0.021	1.506
	Sonication at 106 W/L	3.833	0.996	0.049	2.208
	Sonication at 199 W/L	5.000	0.998	0.040	1.392
	Sonication at 279 W/L	5.833	0.999		0.831

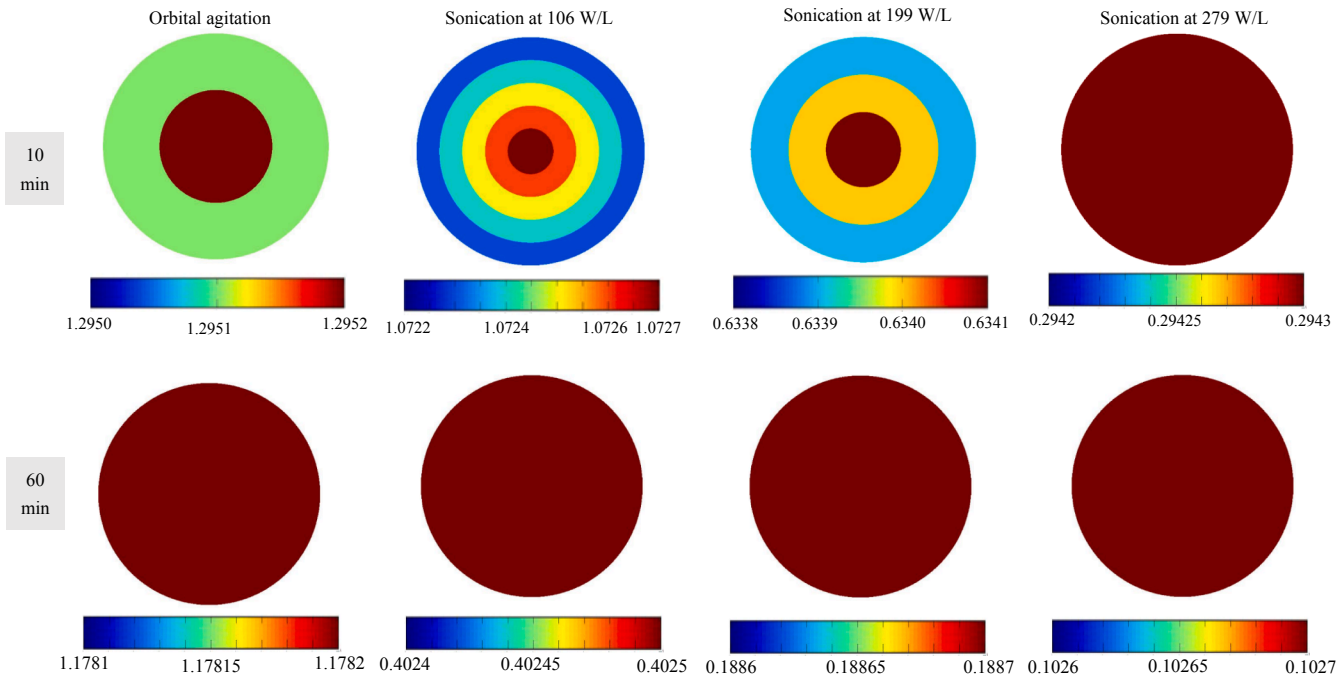

Fig. 7. Distribution of total anthocyanin concentration (mg/cm^3) along with the radial direction of macroporous resins during desorption at 20 °C.

Moreover, the distributions of anthocyanin content along with the radial direction of macroporous resins during desorption at 20 °C are exhibited in Fig. 7 using the modeling results. As can be seen, there was a concentration gradient at the early stage of desorption, whereas anthocyanins distributed homogeneously at the end of desorption. After desorption for 10 min, anthocyanin concentration gradients within resin particles under orbital agitation and sonication at 279 W/L were smaller than those in resin particles under sonication at 106 and 199 W/L. Similar to the extraction process, the early period of desorption was dominated by the simple washing of anthocyanins located on the external surface of macroporous resins [43]. In this circumstances, both orbital agitation and sonication at high intensities can provide stronger mechanical forces to detach anthocyanins from resin particles than sonication at low intensities, promoting anthocyanins distributed more homogenously.

4. Conclusion

The major task of this work was to explore the mechanism about ultrasound enhancement of adsorption/desorption of anthocyanins using macroporous resins as adsorbent through phenomenological modeling. For this purpose, the *PVSDM* model incorporating the changes of particle size and surface area of resins was qualified to model the anthocyanin adsorption process. The modeling results revealed that ultrasound enhanced both external mass transfer and surface diffusion to facilitate the anthocyanin adsorption process. The D_s values under sonication at 279 W/L and 20 °C was 120% higher than the counterpart under orbital agitation. Interestingly, pore volume diffusion dominated the overall intraparticle diffusion of anthocyanins. However, sonication can weaken the influence of pore volume diffusion, as well as enhance the contribution of surface diffusion to the overall diffusion. Besides, the general diffusion model accurately predicted the changes of anthocyanin desorption capacity. Anthocyanin diffusivity increased with the increases of ultrasound energy and desorption temperature. High-intensity ultrasound also made the distribution of anthocaynins more homogeneously inside macroporous resins during desorption.

Overall, the aforementioned experimental and mathematical investigations enriched the fundamental knowledge about the ultrasound enhancement of adsorption/desorption processes. These results can provide guidance for intelligent control of anthocyanin adsorption/desorption processes in the presence of sonication. Moreover importantly, this work can have a real application for comprehension of phenomena that will permit to apply ultrasound technology in anthocyanin-related food processing, especially in juice and wine industries facing the problems of utilizing byproducts rich in anthocyanins.

Acknowledgements

This work was sponsored by Jiangsu Agricultural Science and Technology Innovation Fund (No. CX(18)2017); National Natural Science Foundation of China (No. 31701616); Natural Science

Foundation of Jiangsu, China (No. BK20170714); Fundamental Research Funds for the Central Universities, China (No. KJQN201824).

Appendix A. Supplementary data

Supplementary data to this article can be found online at https://doi.org/10.1016/j.cej.2019.122530.

References

[1] M.T. Fernández-Ponce, B.R. Parjikolaei, H.N. Lari, L. Casas, C. Mantell, E.J.M. Ossa, Pilot-plant scale extraction of phenolic compounds from mango leaves using different green techniques: KINETIC and scale up study, Chem. Eng. J. 299 (2016) 420–430, https://doi.org/10.1016/j.cej.2016.04.046.

[2] O. Gligor, A. Mocan, C. Moldovan, M. Locatelli, G. Crișan, I.C.F.R. Ferreira, Enzyme-assisted extractions of polyphenols – a comprehensive review, Trends Food Sci. Technol. 88 (2019) 302–315, https://doi.org/10.1016/j.tifs.2019.03.029.

[3] Y. Tao, D. Wu, Q.-A. Zhang, D.-W. Sun, Ultrasound-assisted extraction of phenolics from wine lees: modeling, optimization and stability of extracts during storage, Ultrason. Sonochem. 21 (2014) 706–715, https://doi.org/10.1016/j.ultsonch.2013.09.005.

[4] G. Aragones, F. Danesi, D.D. Rio, P. Mena, The importance of studying cell metabolism when testing the bioactivity of phenolic compounds, Trends Food Sci. Tech. 69 (2017) 230–242, https://doi.org/10.1016/j.tifs.2017.02.001.

[5] C.A. Perussello, Z. Zhang, A. Marzocchella, B.K. Tiwari, Valorization of apple pomace by extraction of valuable compounds, Compr. Rev. Food Sci. Food Saf. 16 (2017) 776–796, https://doi.org/10.1111/1541-4337.12290.

[6] Z. Fang, B. Bhandari, Encapsulation of polyphenols – a review, Trends Food Sci. Technol. 21 (2010) 510–523, https://doi.org/10.1016/j.tifs.2010.08.003.

[7] T.J. Buran, A.K. Sandhu, Z. Li, C.R. Rock, W.W. Yang, L. Gu, Adsorption/desorption characteristics and separation of anthocyanins and polyphenols from blueberries using macroporous adsorbent resins, J. Food Eng. 128 (2014) 167–173, https://doi.org/10.1016/j.jfoodeng.2013.12.029.

[8] M.L. Soto, A. Moure, H. Domínguez, J.C. Parajó, Recovery, concentration and purification of phenolic compounds by adsorption: a review, J. Food Eng. 105 (2011) 1–27, https://doi.org/10.1016/j.jfoodeng.2011.02.010.

[9] L. Wang, N. Boussetta, N. Lebovka, E. Vorobiev, Ultrasound assisted purification of polyphenols of apple skins by adsorption/desorption procedure, Ultrason. Sonochem. 55 (2019) 18–24, https://doi.org/10.1016/j.ultsonch.2019.03.002.

[10] D.P. Zagklis, C.A. Paraskeva, Purification of grape marc phenolic compounds through solvent extraction, membrane filtration and resin adsorption/desorption, Sep. Purif. Technol. 156 (2015) 328–335, https://doi.org/10.1016/j.seppur.2015.10.019.

[11] F. Chemat, Z. Huma, M.K. Khan, Applications of ultrasound in food technology: processing, preservation and extraction, Ultrason. Sonochem. 18 (2011) 813–835, https://doi.org/10.1016/j.ultsonch.2010.11.023.

[12] Y. Picó, Ultrasound-assisted extraction for food and environmental samples, Trends Anal. Chem. 43 (2013) 84–99, https://doi.org/10.1016/j.trac.2012.12.005.

[13] O. Hamdaoui, E. Naffrechoux, L. Tifouti, C. Pétrier, Effects of ultrasound on adsorption-desorption of p-chlorophenol on granular activated carbon, Ultrason. Sonochem. 10 (2003) 109–114, https://doi.org/10.1016/S1350-4177(02)00137-2.

[14] G. Jing, Z. Zhou, L. Song, M. Dong, Ultrasound enhanced adsorption and desorption of chromium (VI) on activated carbon and polymeric resin, Desalination 279 (2011) 423–427, https://doi.org/10.1016/j.desal.2011.06.001.

[15] S.K. Low, M.C. Tan, N.L. Chin, Effect of ultrasound pre-treatment on adsorbent in dye adsorption compared with ultrasound simultaneous adsorption, Ultrason. Sonochem. 48 (2018) 64–70, https://doi.org/10.1016/j.ultsonch.2018.05.024.

[16] Y. Wu, Y. Han, Y. Tao, S. Fan, D.-T. Chu, X. Ye, M. Ye, G. Xie, Ultrasound assisted adsorption and desorption of blueberry anthocyanins using macroporous resins, Ultrason Sonochem. 48 (2018) 311–320, https://doi.org/10.1016/j.ultsonch.2018.06.016.

[17] K.Y. Foo, B.H. Hameed, Insights into the modeling of adsorption isotherm systems, Chem. Eng. J. 156 (2010) 2–10, https://doi.org/10.1016/j.cej.2009.09.013.

[18] G.Z. Kyzas, N.K. Lazaridis, M. Kostoglou, Adsorption/desorption of a dye by a chitosan derivative: experiments and phenomenological modeling, Chem. Eng. J. 248 (2014) 327–336, https://doi.org/10.1016/j.cej.2014.03.063.

[19] P.Y.R. Suzaki, M.T. Munaro, C.C. Triques, S.J. Kleinübing, M.R.F. Klen, L.M.M. Jorge, R. Bergamasco, Biosorption of binary heavy metal systems: phenomenological mathematical modeling, Chem. Eng. J. 313 (2017) 364–373, https://doi.org/10.1016/j.cej.2016.12.082.

[20] Q. Zhu, G. Moggridge, C. D'Agostino, Adsorption of pyridine from aqueous solutions by polymeric adsorbents MN 200 and MN 500. Part 2: kinetics and diffusion analysis, Chem. Eng. J. 306 (2016) 1223–1233, https://doi.org/10.1016/j.cej.2016.07.087.

[21] V. Díaz-Blancas, R. Ocampo-Pérez, R. Leyva-Ramos, P.A. Alonso-Dávila, A.I. Moral-Rodríguez, 3D modeling of the overall adsorption rate of metronidazole on granular activated carbon at low and high concentrations in aqueous solution, Chem. Eng. J. 349 (2018) 82–91, https://doi.org/10.1016/j.cej.2018.05.076.

[22] G.L. Dotto, C. Buriol, L.A.A. Pinto, Diffusional mass transfer model for the adsorption of food dyes on chitosan films, Chem. Eng. Res. Des. 92 (2014) 2324–2332, https://doi.org/10.1016/j.cherd.2014.03.013.

[23] R. Ocampo-Perez, R. Leyva-Ramos, P. Alonso-Davila, J. Rivera-Utrilla, M. Sanchez-Polo, Modeling adsorption rate of pyridine onto granular activated carbon, Chem. Eng. J. 165 (2010) 133–141, https://doi.org/10.1016/j.cej.2010.09.002.

[24] Z. Rogala, P. Kolasiński, Z. Gnutek, Modelling and experimental analyzes on air-fluidised silica gel-water adsorption and desorption, Appl. Therm. Eng. 127 (2017) 950–962, https://doi.org/10.1016/j.applthermaleng.2017.07.122.

[25] A.C. Fröhlich, R. Ocampo-Pérez, V. Diaz-Blancas, N.P.G. Salau, G.L. Dotto, Three-dimensional mass transfer modeling of ibuprofen adsorption on activated carbon prepared by sonication, Chem. Eng. J. 341 (2018) 65–74, https://doi.org/10.1016/j.cej.2018.02.020.

[26] M. Ondarts, L. Reinert, S. Guittonneau, S. Baup, S. Delpeux, J. Lévêque, L. Duclaux, Improving the adsorption kinetics of ibuprofen on an activated carbon fabric through ultrasound irradiation: simulation and experimental studies, Chem. Eng. J. 343 (2018) 163–172, https://doi.org/10.1016/j.cej.2018.02.062.

[27] Y. Tao, Y. Han, W. Liu, L. Peng, Y. Wang, S. Kadam, P.L. Show, X. Ye, Parametric and phenomenological studies about ultrasound-enhanced biosorption of phenolics from fruit pomace extract by waste yeast, Ultrason. Sonochem. 52 (2019) 193–204, https://doi.org/10.1016/j.ultsonch.2018.11.018.

[28] V. Ivanova, Á. Dörnyei, L. Márk, B. Vojnoski, T. Stafilov, M. Stefova, F. Kilár, Polyphenolic content of Vranec wines produced by different vinification conditions, Food Chem. 124 (2011) 316–325, https://doi.org/10.1016/j.foodchem.2010.06.039.

[29] G.L. Dotto, L.A.A. Pinto, Analysis of mass transfer kinetics in the biosorption of synthetic dyes onto Spirulina platensis nanoparticles, Biochem. Eng. J. 68 (2012) 85–90, https://doi.org/10.1016/j.bej.2012.07.010.

[30] R. Leyva-Ramos, J. Rivera-Utrilla, N.A. Medellin-Castillo, M. Sanchez-Polo, Kinetic modeling of fluoride adsorption from aqueous solution onto bone char, Chem. Eng. J. 158 (2010) 458–467, https://doi.org/10.1016/j.cej.2010.01.019.

[31] V. Ponnusami, K.S. Rajan, S.N. Srivastava, Application of film-pore diffusion model for methylene blue adsorption onto plant leaf powders, Chem. Eng. J. 163 (2010) 236–242, https://doi.org/10.1016/j.cej.2010.07.052.

[32] T. Furusawa, J.M. Smith, Fluid-particle and intraparticle mass transport rates in slurries, Ind. Eng. Chem. Fundam. 12 (1973) 197–203, https://doi.org/10.1021/i160046a009.

[33] J. Adamíková, M. Antošová, M. Polakovič, A method of early phase selection of carrier for Aspergillus Oryzae β-galactosidase immobilization for galactooligosaccharides production, Biotechnol J. 1800120 (2018), https://doi.org/10.1002/biot.201800120.

[34] H. Komiyama, J.M. Smith, Intraparticle mass transport in liquid-filled pores, AICHE J. 20 (1974) 728–734, https://doi.org/10.1002/aic.690200414.

[35] M. Monsanto, T. Radhakrishnan, D. Sevillano, N. Hooshyar, J. Meuldijk, E. Zondervan, Modeling and Optimization of an Adsorption Process for the Recovery of Catechins from Green Tea, Proceedings of the 24th European Symposium on Computer Aided Process Engineering, Jiří Jaromír Klemeš, Petar Sabev Varbanov and Peng Yen Liew Ed. (2014) 1441–1446. https://doi.org/10.1016/B978-0-444-63455-9.50075-1.

[36] M. Barrande, R. Bouchet, R. Denoyel, Tortuosity of porous particles, Anal. Chem. 79 (2007) 9115–9121, https://doi.org/10.1021/ac071377r.

[37] C.R. Wilke, P. Chang, Correlation of diffusion coefficients in dilute solutions, AICHE J. 1 (1955) 264–270, https://doi.org/10.1002/aic.690010222.

[38] M. Otero, M. Zabkova, A.E. Rodrigues, Phenolic wastewaters purification by thermal parametric pumping: modeling and pilot-scale experiments, Water Res. 39 (2005) 3467–3478, https://doi.org/10.1016/j.watres.2005.06.016.

[39] C. Mantell, M. Rodríguez, E.M.D.L. Ossa, Semi-batch extraction of anthocyanins from red grape pomace in packed beds: experimental results and process modeling, Chem. Eng. Sci. 57 (2002) 3831–3838, https://doi.org/10.1016/S0009-2509(02)00320-2.

[40] M. Cissé, P. Bohuon, F. Sambe, C. Kane, M. Sakho, M. Dornier, Aqueous extraction of anthocyanins from *Hibiscus sabdarif* a: experimental kinetics and modeling, J. Food Eng. 109 (2012) 16–21, https://doi.org/10.1016/j.jfoodeng.2011.10.012.

[41] J.V. Garcia-Perez, M.A. García-Alvarado, J.A. Carcel, A. Mulet, Extraction kinetics modeling of antioxidants from grape stalk (*Vitis vinifera* var. Bobal): Influence of drying conditions, J. Food Eng. 101 (2010) 49–58, https://doi.org/10.1016/j.jfoodeng.2010.06.008.

[42] J.G. Gujar, S.J. Wagh, V.G. Gaikar, Experimental and modeling studies on microwave-assisted extraction of thymol from seeds of *Trachyspermum ammi* (TA), Sep. Purif. Technol. 70 (2010) 257–264, https://doi.org/10.1016/j.seppur.2009.08.005.

[43] Y. Tao, Z. Zhang, D.-W. Sun, Experimental and modeling studies of ultrasound-assisted release of phenolics from oak chips into model wine, Ultrason. Sonochem. 21 (2014) 1839–1848, https://doi.org/10.1016/j.ultsonch.2014.03.016.

[44] P.R. Gogate, A.B. Pandit, Engineering design method for cavitational reactors: I. Sonochemical reactors, AICHE J. 46 (2000) 372–379, https://doi.org/10.1002/aic.690460215.

[45] M. Wang, W. Yuan, Modeling bubble dynamics and radical kinetics in ultrasound induced microalgal cell disruption, Ultrason. Sonochem. 28 (2016) 7–14, https://doi.org/10.1016/j.ultsonch.2015.06.025.

[46] Y. Kohno, E. Haga, K. Yoda, M. Shibata, C. Fukuhara, Adsorption behavior of natural anthocyanin dye on mesoporous silica, J. Phys. Chem. Solids 75 (2014) 48–51, https://doi.org/10.1016/j.jpcs.2013.08.007.

[47] Z.-S. Zhang, L.-J. Wang, D. Li, S.-S. Jiao, X.D. Chen, Z.-H. Mao, Ultrasound-assisted

extraction of oil from flaxseed, Sep. Purif. Technol. 62 (2008) 192–198, https://doi.org/10.1016/j.seppur.2008.01.014.
[48] D. Liu, X.-A. Zeng, D.-W. Sun, Z. Han, Disruption and protein release by ultrasonication of yeast cells, Innov. Food Sci. Emerg. Technol. 18 (2013) 132–137, https://doi.org/10.1016/j.ifset.2013.02.006.
[49] L. Qiao, X. Ye, Y. Sun, J. Ying, Y. Shen, J. Chen, Sonochemical effects on free phenolic acids under ultrasound treatment in a model system, Ultrason. Sonochem. 20 (2013) 1017–1025, https://doi.org/10.1016/j.ultsonch.2012.12.007.
[50] Y. Tao, Y. Wang, M. Pan, S. Zhong, Y. Wu, R. Yang, Y. Han, J. Zhou, Combined ANFIS and numerical methods to simulate ultrasound assisted extraction of phenolics from chokeberry cultivated in China and analysis of phenolic composition, Sep. Purif. Technol. 178 (2017) 178–188, https://doi.org/10.1016/j.seppur.2017.01.012.
[51] W.-N. Zhang, H.-L. Zhang, C.-Q. Lu, J.-P. Luo, X.-Q. Zha, A new kinetic model of ultrasound-assisted extraction of polysaccharides from Chinese chive, Food Chem. 212 (2016) 274–281, https://doi.org/10.1016/j.foodchem.2016.05.144.